ISSN 1027-4510, Journal of Surface Investigation: X-ray, Synchrotron and Neutron Techniques, 2023, Vol. 17, No. 3, pp. 620–624. © Pleiades Publishing, Ltd., 2023.

Investigation of Electronic and Atomic Structure and Transport Properties of Black Phosphorus Single Crystals

S. V. Chekmazov[a], *, A. A. Zagitova[a], A. M. Ionov[a], S. G. Protasova[a], V. N. Zverev[a], A. A. Mazilkin[a], V. I. Kulakov[a], and S. I. Bozhko[a], **

[a] *Institute of Solid State Physics, Russian Academy of Sciences, Chernogolovka, 142432 Russia*

**e-mail: chekmazov@issp.ac.ru*

***e-mail: bozhko@issp.ac.ru*

Received October 15, 2022; revised December 21, 2022; accepted December 21, 2022

Abstract—The electronic and atomic structure and transport properties of black phosphorus single crystals prepared by high-pressure and gas-transport methods were studied by X-ray photoelectron spectroscopy and scanning probe microscopy (STM, AFM). The atomic resolution of the single crystal surface was obtained by scanning tunneling microscopy. After exposure of the clean surface under ambient conditions, the features in X-ray photoelectron spectroscopy spectra corresponding to the oxidized form of phosphorus were observed and detected using atomic force microscopy. Using low-temperature transport measurements, impurity activation energies were determined and negative magnetoresistance was detected.

Keywords: materials science, crystal growth, black phosphorus (bP), nanoislands, scanning tunneling microscopy (STM), scanning tunneling spectroscopy (STS), atomic force microscopy (AFM), density functional theory (DFT), X-ray photoelectron spectroscopy (XPS), magnetoresistance, weak localization

DOI: 10.1134/S1027451023030035

INTRODUCTION

Recently, in condensed-matter physics, greater attention has been paid to systems with reduced dimensionality. Among two-dimensional materials monoatomic layers of elements have also been studied and black phosphorus (bP) single crystal, the allotropic modification of phosphorus [1–3], has been proposed as a promising material.

In the bP crystal, atomic layers are bonded by weak van der Waals forces. The atomic layers of bP have a "corrugated" structure in contrast to graphene. The lattice belongs to orthorhombic syngony with an interlayer gap of about 5.3 Å. In the bP monolayer, two types of bonds are presented: a short bond of 2.224 Å connects the nearest P atoms in one plane, a longer bond of 2.244 Å connects the upper and lower atoms of the layer [4].

The anisotropic structure of bP determines its anisotropic physical properties and distinguishes it among two-dimensional materials. The first experiments were carried out on polycrystalline samples. bP was determined to be a *p*-type direct-band semiconductor with a band gap of 0.33–0.35 eV [5–8]. According to theoretical calculations [9–11], the minimum of the conduction band and the maximum of the valence band (VB) are located at the *Z*-point of the Brillouin zone. With a decrease in the number of layers, the width of the gap at the *T*-point increases and for phosphorene, reaches 1.5–2 eV [12]. The bP remains a direct-gap semiconductor, which distinguishes it from metal dichalcogenides, where the gap becomes indirect with a decreasing number of layers.

The first methods of obtaining bP crystals did not allow the synthesis of large single crystals [13–15]. The method of gas-transport reaction [16–18] produced single crystals, but the results vary depending on the synthesis conditions, and the growth mechanisms have not been fully revealed yet. Therefore, one of the goals of the work was to prepare large bP single crystals. The morphology, atomic and electronic structure of the crystal surface, and low-temperature electrical conductivity and magnetoresistance of the samples were studied.

RESULTS AND DISCUSSION

Single crystals were obtained by two methods. In the high-pressure method, red phosphorus was placed in the pyrophylitic ampoule of a high-pressure container, the synthesis was carried out at pressure $P =$ 1.1 GPa and temperature $T = 860$°C. In the gas-transport reaction method, red phosphorus, AuSn and SnI_4 were placed in a 10-cm-long quartz ampoule at $p =$

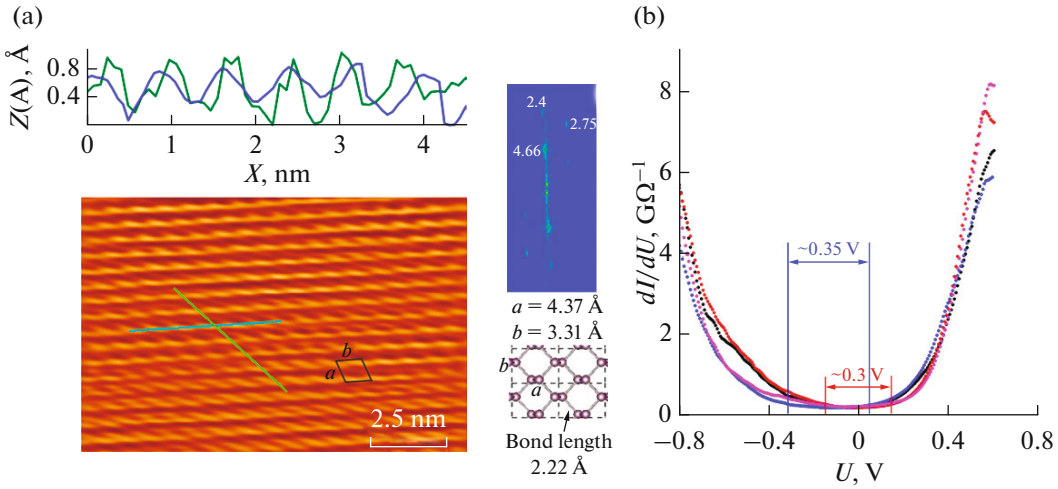

Fig. 1. STM image of the bP (100) surface (insets: profiles along the lines (a), FFT of the STM image (reflexes are indicated in Å), unit cell image), STS spectra taken at four different points (b).

10^{-2} Torr and kept at temperature T = 590°C. The temperature gradient along the ampoule was 10–20°C and single crystals grew up at the colder end of the ampoule for 5 days. The bP crystal had an orthorhombic crystal structure with space group Cmca, a = 4.37 Å, b = 3.31 Å, c = 10.47 Å, the X-ray data confirmed crystallinity of the samples. Crystals with dimensions of 10 × 20 μm^2 were obtained by the high-pressure method, those obtained using the gas-transport reaction method were of 1 mm × 100 μm. The crystal growth during the gas-transport reaction occurred along the Y direction.

The investigation of the surface was carried out by STM in ultrahigh vacuum (pressure was 10^{-10} Torr) and by AFM in the air. The sample was split by a sticky tape in vacuum of 10^{-8} Torr. The STM image of the bP(100) surface acquired at U_{bias} = + 0.6 V, I_{tun} = 100 pA is presented in Fig. 1a. The atomic resolution was obtained at T = 300 K. The Fourier transform of the STM image shows the presence of a long-range order. The lattice parameters a = 4.66 Å and b = 2.75 Å obtained from the Fourier analysis are close to those obtained from the X-ray diffraction analysis.

Figure 1b shows the tunnel spectra recorded at four points of the sample (T = 300 K). The band gap estimated from the spectra is 0.3–0.35 eV is in accordance with [3, 5].

The elemental composition and electronic structure of the P(100) were investigated by XPS (AlK_α-radiation h_ν = 1486.6 eV). The XPS spectrum of the bP surface is shown in Fig. 2a. The core level spectra of P 2s and P 2p characteristic of pure phosphorus were observed (Fig. 2c). No impurities were found on the bP surface after the synthesis.

Stability of the bP surface under various conditions was studied by XPS. The XPS spectra of a clean surface, obtained after ion etching and aged under atmospheric conditions for a period from several hours to 100 days, were taken. In the spectrum of an as-grown sample there is a spin-orbit doublet of P 2$p_{1/2}$ and P 2$p_{3/2}$ with binding energies (BE) of 131.1 and 130.2 eV (Fig. 2c), characteristic of pure phosphorus.

Surface exposure in the air leads to a doublet shift towards higher BE by 0.25 eV, the spin-orbit splitting has not changed, that agrees with [19]. Moreover, an additional peak corresponding to the oxide form of phosphorus, presumably P_2O_5, was detected at 135 eV. Also, nanoislands about 5 nm in height and 50 nm in width (Fig. 2d) were found by AFM after exposure of the surface in the air for several days. According to [20], the nanoislands, represent oxidized sections of the phosphorus surface.

Using XPS, the VB structure was studied. Figure 2b demonstrates the VB spectra for a pure and oxidized surface of bP crystals. In the spectrum of the pure bP surface, features are presented at BE of 2.8, 5, 6.5, 11, and 14 eV. The spectrum of a sample maintained under atmospheric conditions demonstrated that peaks with BE of 2.8, 5, and 6.5 eV corresponding to bP are suppressed, and features in the range of 5–12 eV appear related to the phosphorus oxidized form.

To justify the experimental data, calculation of the density of states (DOS) was carried out using density functional method (DFT) (the lower curve in Fig. 2b). Crystal structure and DOS were investigated using Vienna Ab-initio Simulation Package software. The unit cell contains a vacuum gap of 15 Å, designed to reduce the influence of neighboring stacks on each other, allowing us to simulate the structure of thin

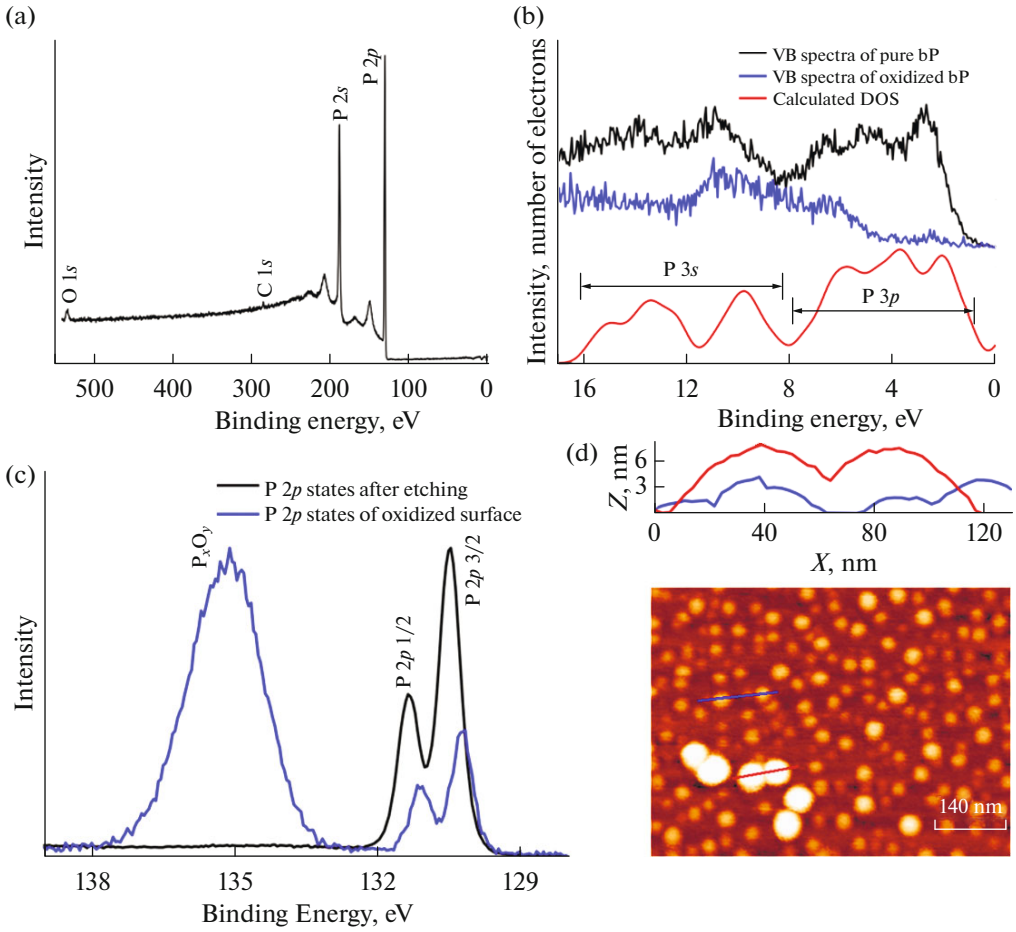

Fig. 2. XPS spectrum of the bP(100) synthesized by high-pressure method after etching (a). VB spectra and calculated DOS (b). P 2*p* states spectra after etching and exposure under atmospheric conditions for 100 days (c). AFM image of the oxidized bP surface (inset: profiles along the lines) (d).

films. The lattice parameters of bP obtained after geometric optimization ($a = 4.46$ Å, $b = 3.34$ Å, $c = 10.71$ Å) are close to the experimental data. For calculation of the electronic structure, the optPBE-vdW functional, $E_{cutoff} = 520$ eV and a 12 × 12 × 10 Monkhorst-Pack sampling grid were used. The main contribution to the DOS in the range from 8 to 16 eV is made by 3s states, and in the range of 1–8 eV it is made by 3p states. The results obtained qualitatively are consistent with [9–11].

For transport measurements, larger single crystals obtained by the gas-transport method were used. The electrical resistance measurements of samples 1 and 2 were carried out with direct current by a four-contact method, the electrical conductivity and magnetoresistance of sample 3 were measured with alternating current. The current direction coincided with the *Y* direction. Figure 3a shows the temperature dependence of the crystal resistance in a range 4.2–300 K.

The temperature range below 300 K corresponds to the impurity conductivity, and the resistance increases exponentially with an increasing temperature. The activation energy of the impurities, calculated from the temperature dependence of the resistance, was 10, 16 and 7 meV for samples 1, 2 and 3, respectively, which agrees with [8]. Figure 3b shows the temperature dependence of the electrical conductivity of sample 3 from 1.5 to 10 K.

The temperature dependence of the electrical conductivity of sample 3 is linear in a logarithmic scale, which is characteristic of the weak localization regime in the two-dimensional case. The results are in an agreement with [21], where two-dimensional contribution to the conductivity is observed.

Weak localization was detected by its destruction in a magnetic field due to a gradual decrease in the interference corrections to the resistivity. Figure 3c shows magnetoresistance measurements at $T = 0.5$ K in a magnetic field of up to 8 T. The direction of the current coincided with the *Y* direction, the magnetic field was applied perpendicular to the layer planes along *Z*

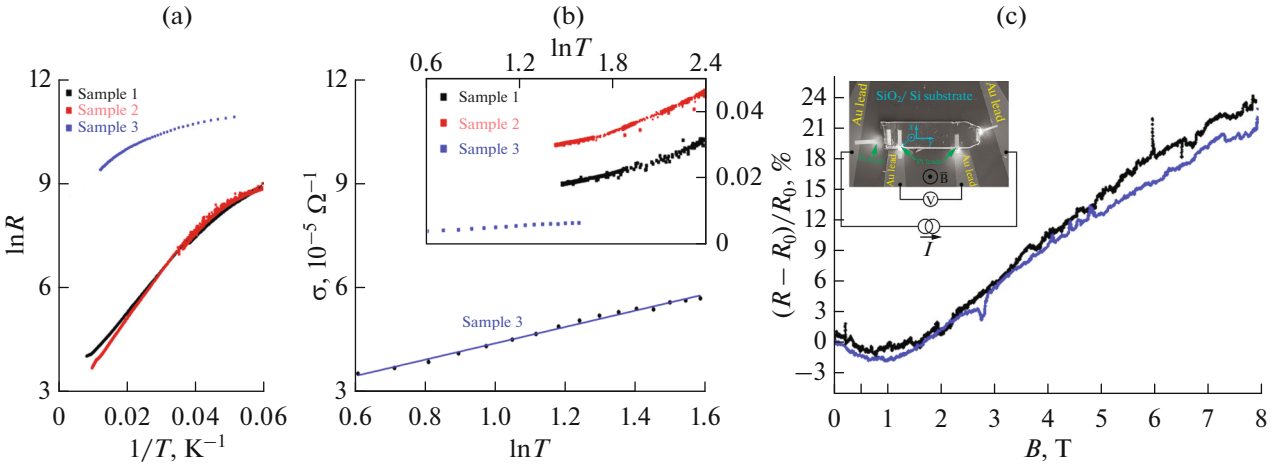

Fig. 3. Temperature dependences of the resistance/conductivity (a/b) of the samples. Dependence of the magnetoresistance of the sample 3 on an applied magnetic field (black—the magnetic field increases, blue—the magnetic field decreases) (inset: SEM image of the sample with Pt electrical leads for a standard four-point technique measurement) (c).

direction. Note that magnetoresistance reaches its minimum at $B_{min} = 0.95$ T. At greater fields, a complete destruction of weak localization apparently takes place, and the resistance increases with the field. The electron mean free path calculated from B_{min} was about 260 Å. The maximum of the negative magnetoresistance was 1.8% at a field of 0.95 T.

CONCLUSIONS

The conditions for synthesis of bP crystals have been optimized, and single crystals have been obtained by high-pressure and gas-transport methods. The electronic structure has been studied by XPS, and the experimental data have been confirmed by DFT simulations. The atomic resolution of the crystal surface has been obtained by STM. The band gap estimation (0.3–0.35 eV) for bP has been made from the STS spectra. The oxidized islands detected by AFM indicate oxidation of the bP surface exposed in the air.

From the linear nature of the electrical conductivity dependence on temperature in the logarithmic scale below 10 K and the presence of negative magnetoresistance at 0.5 K in magnetic fields from 0 to 0.95 T, it is assumed that a weak localization effect is observed in the two-dimensional case under these conditions.

ACKNOWLEDGMENTS

The authors are grateful to the Research Facility Center of ISSP RAS for technical support. The support of Funding of the State task for ISSP RAS is gratefully acknowledged.

CONFLICTS OF INTEREST

The authors confirm that they have no conflicts of interest to declare that are relevant to the content of this article.

REFERENCES

1. H. Liu, A. T. Neal, Z. Zhu, Z. Luo, X. Xu, D. Tomanek, and P. D. Ye, ACS Nano **8**, 4033 (2014). https://doi.org/10.1021/nn501226z
2. J. Qiao, X. Kong, Z.-X. Hu, F. Yang, and W. Ji, Nat. Commun. **5**, 4475 (2014). https://doi.org/10.1038/ncomms5475
3. L. Li, Yu. Y., G. J. Ye, Q. Ge, X. Ou, H. Wu, D. Feng, X. H. Chen, and Y. Zhang, Nat. Nanotechnol. **9**, 372 (2014). https://doi.org/10.1038/nnano.2014.35
4. A. Morita, Appl. Phys. A **39**, 227 (1986). https://doi.org/10.1007/BF00617267
5. R. W. Keyes, Phys. Rev. **92**, 580 (1953). https://doi.org/10.1103/PhysRev.92.580
6. D. Warschauer, J. Appl. Phys. **34**, 1853 (1963). https://doi.org/10.1063/1.1729699
7. Y. Akahama, S. Endo, and S.-I. Narita, J. Phys. Soc. Jpn. **52**, 2148 (1983). https://doi.org/10.1143/JPSJ.52.2148
8. M. Baba, Y. Nakamura, Y. Takeda, K. Shibata, A. Morita, Y. Koike, and T. Fukase, J. Phys.: Condens. Matter **4**, 1535 (1992). https://doi.org/10.1088/0953-8984/4/6/018
9. Y. Takao, H. Asahina, and A. Morita, J. Phys. Soc. Jpn. **50**, 3362 (1981). https://doi.org/10.1143/JPSJ.50.3362
10. N. B. Goodman, L. Ley, and D. W. Bullett, Phys. Rev. B **27**, 7440 (1983). https://doi.org/10.1103/PhysRevB.27.7440
11. Y. Cai, G. Zhang, and Y.-W. Zhang, Sci. Rep. **4**, 6677 (2014). https://doi.org/10.1038/srep06677

12. L. Liang, J. Wang, W. Lin, B. G. Sumpter, V. Meunier, and M. Pan, Nano Lett. **14**, 6400 (2014). https://doi.org/10.1021/nl502892t
13. P. W. Bridgman, J. Am. Chem. Soc. **36**, 1344 (1914). https://doi.org/10.1021/ja02184a002
14. H. Krebs, H. Weitz, and K. H. Worms, Z. Anorg. Allg. Chem. **280**, 119 (1955). https://doi.org/10.1002/zaac.19552800110
15. A. Brown and S. Rundqvist, Acta Crystallogr. **19**, 684 (1965). https://doi.org/10.1107/S0365110X65004140
16. S. Lange, P. Schmidt, and T. Nilges, Inorg. Chem. **46**, 4028 (2007). https://doi.org/10.1021/ic062192q
17. T. Nilges, M. Kersting, and T. Pfeifer, J. Solid State Chem. **181**, 1707 (2008). https://doi.org/10.1016/j.jssc.2008.03.008
18. M. Kopf, N. Eckstein, D. Pfister, C. Grotz, I. Kruger, M. Greiwe, T. Hansen, H. Kohlmann, and T. Nilges, J. Cryst. Growth **405**, 6 (2014). https://doi.org/10.1016/j.jcrysgro.2014.07.029
19. M. T. Edmonds, A. Tadich, A. Carvalho, A. Ziletti, K. M. O'Donnell, S. P. Koenig, D. F. Coker, Zyilmaz B., A. H. Castro Neto, and M. S. Fuhrer, ACS Appl. Mater. Interfaces **7**, 14557 (2015). https://doi.org/10.1021/acsami.5b01297
20. J. Kang, J. D. Wood, S. A. Wells, J.-H. Lee, X. Liu, K.-S. Chen, and M. C. Hersam, ACS Nano **9**, 3596 (2015). https://doi.org/10.1021/acsnano.5b01143
21. M. Baba, F. Izumida, Y. Takeda, K. Shibata, A. Morita, Y. Koike, and T. Fukase, J. Phys. Soc. Jpn. **60**, 3777 (1991). https://doi.org/10.1143/JPSJ.60.3777